Supporting Information

$BaYF_5:Yb^{3+},Tm^{3+}$ Upconverting Nanoparticles with Improved Population of the Visible and Near-Infrared Emitting States: Implications for Bioimaging

Steven L. Maurizio[a], Gabriella Tessitore[a], Karl W. Krämer[b], and John A. Capobianco[a]*

[a]Department of Chemistry and Biochemistry & Centre for Nanoscience Research, Concordia University, 7141 Sherbrooke St. W., H4B 1R6, Montreal, Canada

[b]Department of Chemistry and Biochemistry, University of Bern, Freiestrasse 3, 3012 Bern, Switzerland

Email: John.Capobianco@concordia.ca.

Table S1. ICP-MS results for synthesized cubic $Ba_{1-x}Y_xF_{2+x}$ nanoparticles with varying values of x.

Nominal x Value	Y^{3+} (mol)	Ba^{2+} (mol)	Experimental x Value
0.80	$4.62 \times 10^{-6} \pm 9.45 \times 10^{-8}$	$1.87 \times 10^{-6} \pm 2.42 \times 10^{-8}$	0.71 ± 0.12
0.67	$6.03 \times 10^{-5} \pm 6.55 \times 10^{-7}$	$3.71 \times 10^{-5} \pm 5.23 \times 10^{-7}$	0.62 ± 0.15
0.50	$5.73 \times 10^{-6} \pm 6.03 \times 10^{-8}$	$5.34 \times 10^{-6} \pm 6.40 \times 10^{-8}$	0.52 ± 0.10
0.33	$2.66 \times 10^{-6} \pm 2.48 \times 10^{-8}$	$6.10 \times 10^{-6} \pm 3.84 \times 10^{-8}$	0.30 ± 0.08
0.20	$1.48 \times 10^{-6} \pm 2.72 \times 10^{-8}$	$7.97 \times 10^{-6} \pm 4.55 \times 10^{-8}$	0.16 ± 0.07

Equation S1 and S2. Bragg's Law and Interplanar distance equations for cubic crystal structures.[1]

$$\lambda = 2d(sin\theta) \quad (1)$$

$$d = a/\sqrt{(h^2 + k^2 + l^2)} \quad (2)$$

Table S2. Bragg's Law table from Figure 3, using Equations S1 and S2.

Plane	$Ba_{0.20}Y_{0.80}F_{2.80}$			$Ba_{0.33}Y_{0.67}F_{2.67}$		
	θ (°)	d (nm)	a (Å)	θ (°)	d (nm)	a (Å)
(111)	13.37	0.3331	5.7698	13.26	0.3358	5.8168
(200)	15.50	0.2882	5.7649	15.34	0.2912	5.8236
(220)	22.21	0.2038	5.7638	21.96	0.2060	5.8261
(311)	26.29	0.1739	5.7681	26.01	0.1757	5.8258
(222)	27.58	0.1664	5.7634	27.30	0.1679	5.8179
(400)	32.31	0.1441	5.7646	31.92	0.1457	5.8275
(331)	35.60	0.1323	5.7680	35.20	0.1336	5.8249
(420)	36.67	0.1290	5.7683	36.27	0.1302	5.8231
(422)	40.90	0.1176	5.7636	40.35	0.1190	5.8285
(511)	43.98	0.1109	5.7640	43.31	0.1123	5.8352
		Average	5.766(2)		Average	5.825(5)
	$Ba_{0.50}Y_{0.50}F_{2.50}$			$Ba_{0.67}Y_{0.33}F_{2.33}$		
	θ (°)	d (nm)	a (Å)	θ (°)	d (nm)	a (Å)
(111)	13.13	0.3391	5.8734	13.00	0.3424	5.9311
(200)	15.19	0.2940	5.8797	14.99	0.2978	5.9563
(220)	21.70	0.2083	5.8925	21.46	0.2105	5.9552
(311)	25.69	0.1777	5.8934	25.39	0.1797	5.9583
(222)	26.89	0.1703	5.8999	26.59	0.1721	5.9615
(400)	31.50	0.1474	5.8970	31.18	0.1488	5.9514
(331)	34.70	0.1353	5.8981	34.31	0.1367	5.9568
(420)	35.72	0.1319	5.9005	35.29	0.1333	5.9629
(422)	39.79	0.1204	5.8966	39.28	0.1217	5.9605
(511)	42.75	0.1135	5.8966	42.13	0.1148	5.9668
		Average	5.893(9)		Average	5.96(1)

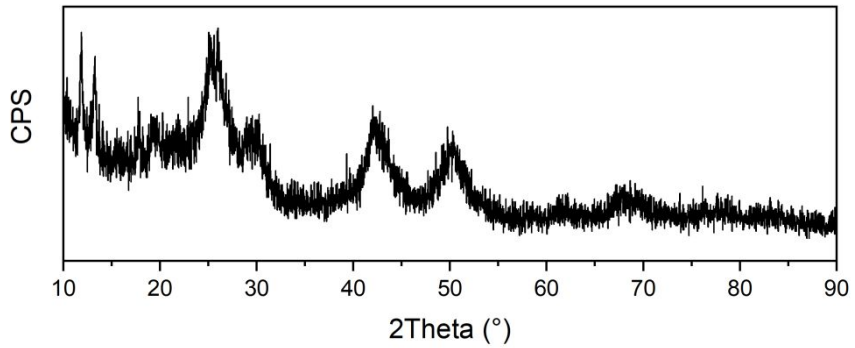

Figure S1. PXRD pattern for synthesized $Ba_{0.8}Y_{0.2}F_{2.2}$ nanoparticles.

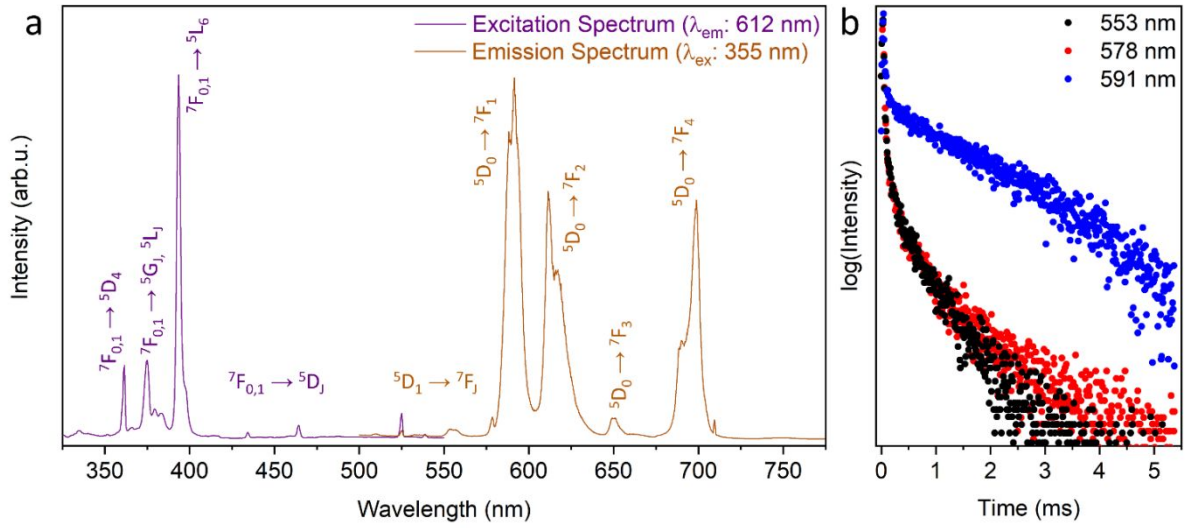

Figure S2. Cubic barium yttrium fluoride nanoparticles doped with Eu^{3+}: (a) excitation (λ_{em} = 612 nm) and emission (λ_{ex} = 355 nm) spectra; (b) luminescence lifetime of the Eu^{3+} emissions at 553 nm ($^5D_1 \rightarrow {}^7F_2$), 591 nm ($^5D_0 \rightarrow {}^7F_1$), and 578 nm.

The Eu^{3+} ion is widely used to probe the site symmetry of lanthanide ions in a crystal host lattice. Luminescence and excitation spectra of cubic phase nanoparticles doped with 15% Eu^{3+} were studied to verify the rare earth site symmetry, presented in **Figure S2**. Eu^{3+} emissions from the $^5D_0$ and $^5D_1$ levels were observed after $^7F_0 \rightarrow {}^5D_4$ excitation at 355 nm (**Figure S2**a).[2] The emission centered at 591 nm corresponds to the $^5D_0 \rightarrow {}^7F_1$ transition, which is electric and magnetic dipole allowed making it largely independent of the local symmetry of Eu^{3+}. Contrarily, the electric dipole $^5D_0 \rightarrow {}^7F_2$ transition observed at 612 nm is hypersensitive and influenced to a greater extent by the local symmetry, coordination number, and crystal field. In **Figure S2**a it is evident that the intensity of the $^5D_0 \rightarrow {}^7F_1$ transition is higher than the $^5D_0 \rightarrow {}^7F_2$ transition. The weaker hypersensitive electric dipole transition indicates a high symmetry of the Eu^{3+} site compared to other fluoride hosts.[2] This supports the conclusion from the X-ray diffraction data (**Figure 1**) that the cubic $Ba_{1-x}Y_xF_{2+x}$ phase was obtained by our synthesis method. Moreover, in **Figure S2**a the band at 578 nm can be attributed to either the $^5D_1 \rightarrow {}^7F_3$ or $^5D_0 \rightarrow {}^7F_0$ transition. The latter transition occurs only if the Eu^{3+} ions occupy a low symmetry site (C_n, C_{nv} and C_s) without inversion center.[2] Luminescence lifetime measurements (**Figure S2**b) of the $^5D_0$ and $^5D_1$ states showed that the emission at 578 nm follows the $^5D_1$ excited state dynamics, and must be the $^5D_1 \rightarrow {}^7F_3$ transition. This further confirms the higher symmetry of the rare earth site.

To assess the symmetry of the occupied site further, it is instructive to compare the structures of CaF_2 and $Ba_{1-x}Y_xF_{2+x}$, where the Ca^{2+} ions are substituted by either Ba^{2+} or Y^{3+}. The centrosymmetric nature of the cation site in fluorite-like structures (O_h symmetry) should impede j-mixing. This would result in extremely weak electric dipole transitions, due to the forbidden nature of these transitions when the occupied site has an inversion center. However, it is well known that distortions can occur by aliovalent substitution. This substitution gives rise to cation vacancies and/or interstitial anions, which compensate the charge imbalance, change the eight-fold coordination, and reduce the site symmetry with respect to the parent O_h symmetry in CaF_2.

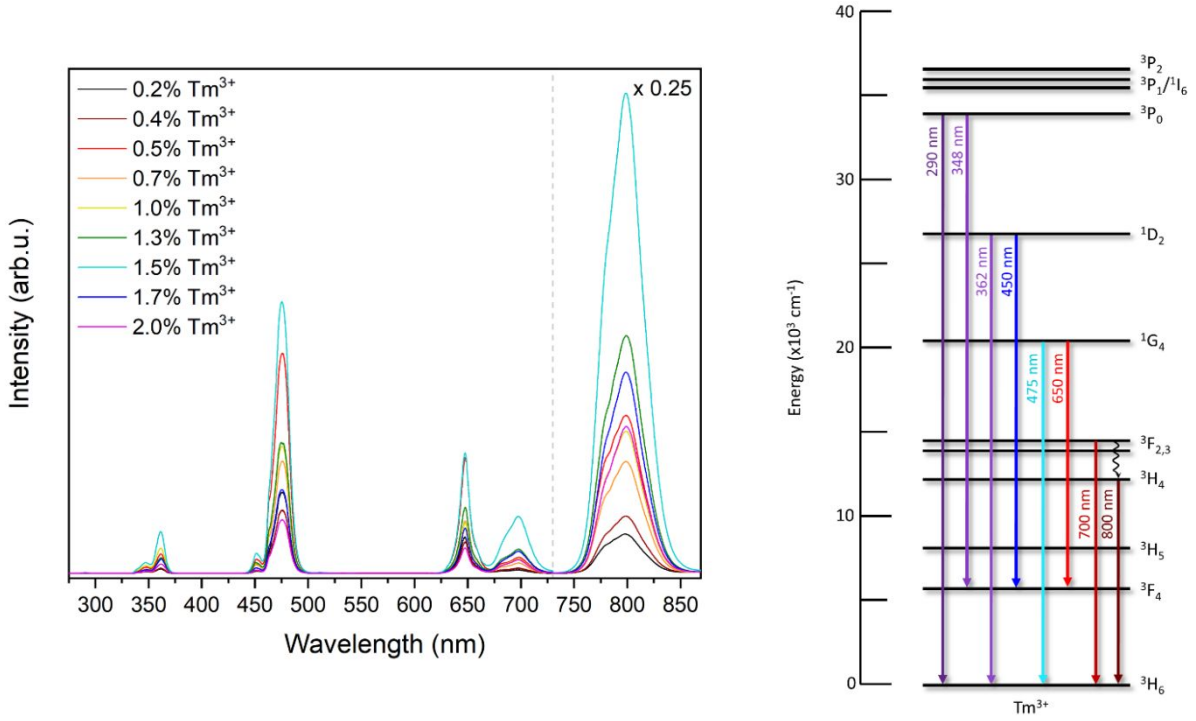

Figure S3. Upconversion emission spectra, upon 976 nm excitation, for $BaYF_5$: 25% Yb^{3+}, x% Tm^{3+} nanoparticles.

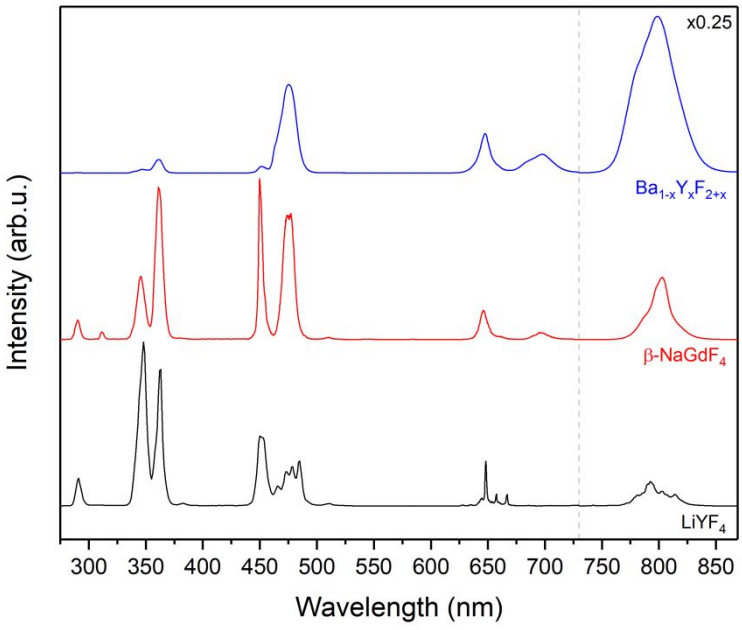

Figure S4. Upconversion emission spectra of $BaYF_5$, β-$NaGdF_4$ and $LiYF_4$ nanoparticles doped with Tm^{3+} and Yb^{3+}.[3,4] Spectra were excited at 976 nm. The NIR spectral range is scaled by x0.25.

Table S3. Crystal structure data, unit cell volume, volume per Y^{3+} ion, and shortest Y^{3+}-Y^{3+} distance for important ternary fluoride host lattices.

	Crystal Phase	Z	Unit Cell Volume (Å^3)	Volume/ Y^{3+} Site (Å^3)	Average Y^{3+}-to-Y^{3+} Distance (Å)*	Ref
$NaYF_4$	Cubic	2	163.7	81.8	5.39	5
$NaYF_4$	Hexagonal	1.5	108.5	72.4	5.17	6
$LiYF_4$	Tetragonal	4	258.3	64.6	4.98	7
$BaYF_5$	Cubic	2	202.3	101.1	5.78	8

*Using the unit cell volume and Z, the volume occupied by each Y^{3+} ion can be calculated. From this value and making the approximation that this volume takes the shape of a sphere, the resulting diameter (from the center of one sphere to the center of an adjacent sphere, 2*r) would be the average distance between Y^{3+} sites.

	Shortest Y^{3+}-Y^{3+} Distance (Å)	Ref.
α-$NaYF_4$	3.87	
β-$NaYF_4$	3.52	6
$LiYF_4$	3.72	9
$BaYF_5$	4.16	10

$\alpha NaYF_4$: $\sqrt{2}\,/\,2 * a = 0.707 * 5.47 = 3.87$
$\beta NaYF_4$: $c = 3.51871$
$LiYF_4$: $(0.25\,a + 0.25\,c)$, *calculated in ICSD*
$BaYF_5$: $\sqrt{2}\,/\,2 * a = 0.707 * 5.89 = 4.16$

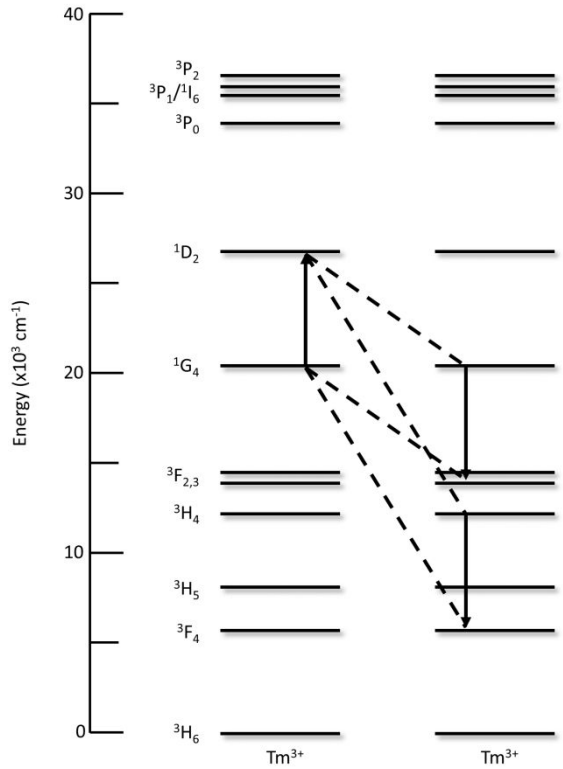

Figure S5. $^1G_4 + {}^3H_4 \rightarrow {}^1D_2 + {}^3F_4$ and $^1G_4 + {}^1G_4 \rightarrow {}^1D_2 + {}^3F_3$ cross-relaxation mechanisms.[11]

Equation S3 and S4. FRET efficiency and Förster distance equations.[12]

$$E_{FRET} = \frac{1}{1 + \left(\frac{r}{R_0}\right)^6} \tag{3}$$

$$R_0 = \sqrt[6]{\frac{3\boldsymbol{\tau_0} c^2 J(\nu)}{8\pi^4 n^2 N'^2 {\nu_0}^2}} \tag{4}$$

Supporting Information References

(1) Suryanarayana, C.; Norton, M. G. *X-Ray Diffraction: A Practical Approach*; Springer US: New York, 1998. https://doi.org/10.1007/978-1-4899-0148-4_1.

(2) Binnemans, K. Interpretation of Europium(III) Spectra. *Coord. Chem. Rev.* **2015**, *295*, 1–45. https://doi.org/10.1016/j.ccr.2015.02.015.

(3) Tessitore, G.; Maurizio, S. L.; Sabri, T.; Capobianco, J. A. Intrinsic Time-Tunable Emissions in Core-Shell Upconverting Nanoparticle Systems. *Angew. Chemie Int. Ed.* **2019**, *58* (29), 9742–9751. https://doi.org/10.1002/anie.201904445.

(4) Maurizio, S. L.; Tessitore, G.; Mandl, G. A.; Capobianco, J. A. Luminescence Dynamics and Enhancement of the UV and Visible Emissions of Tm^{3+} in $LiYF_4$:Yb^{3+},Tm^{3+} Upconverting Nanoparticles. *Nanoscale Adv.* **2019**, *1* (11), 4492–4500. https://doi.org/10.1039/C9NA00556K.

(5) Roy, D. M.; Roy, R. Controlled Massively Defective Crystalline Solutions with the Fluorite Structure. *J. Electrochem. Soc.* **1964**, *111* (4), 421. https://doi.org/10.1149/1.2426145.

(6) Krämer, K. W.; Biner, D.; Frei, G.; Güdel, H. U.; Hehlen, M. P.; Lüthi, S. R. Hexagonal Sodium Yttrium Fluoride Based Green and Blue Emitting Upconversion Phosphors. *Chem. Mater.* **2004**, *16* (7), 1244–1251. https://doi.org/10.1021/cm031124o.

(7) Grzechnik, A.; Syassen, K.; Loa, I.; Hanfland, M.; Gesland, J. Y. Scheelite to Fergusonite Phase Transition in $YLiF_4$ at High Pressures. *Phys. Rev. B* **2002**, *65* (10), 104102. https://doi.org/10.1103/PhysRevB.65.104102.

(8) Gunaseelan, M.; Yamini, S.; Kumar, G. A.; Santhosh, C.; Senthilselvan, J. Photon Upconversion Characteristics of Intense Green Emitting $BaYF_5$:Yb^{3+} ,Er^{3+} Nanoclusters Prepared by Reverse Microemulsion. *Mater. Res. Bull.* **2018**, *107*, 366–378. https://doi.org/10.1016/j.materresbull.2018.08.010.

(9) Goryunov, A. V.; Popov, A. I.; Khajdukov, N. M.; Fedorov, P. P. Crystal Structure of Lithium and Yttrium Complex Fluorides. *Mater. Res. Bull.* **1992**, *27* (2), 213–220. https://doi.org/10.1016/0025-5408(92)90215-L.

(10) Huang, Y.; You, H.; Jia, G.; Song, Y.; Zheng, Y.; Yang, M.; Liu, K.; Guo, N. Hydrothermal Synthesis, Cubic Structure, and Luminescence Properties of $BaYF_5$:RE (RE = Eu, Ce, Tb) Nanocrystals. *J. Phys. Chem. C* **2010**, *114* (42), 18051–18058. https://doi.org/10.1021/jp105061x.

(11) Villanueva-Delgado, P.; Krämer, K. W.; Valiente, R.; de Jong, M.; Meijerink, A. Modeling Blue to UV Upconversion in β-$NaYF_4$:Tm^{3+}. *Phys. Chem. Chem. Phys.* **2016**, *18* (39), 27396–27404. https://doi.org/10.1039/C6CP04347J.

(12) Förster, T. Zwischenmolekulare Energiewanderung Und Fluoreszenz. *Ann. Phys.* **1948**, *437* (1–2), 55–75. https://doi.org/10.1002/andp.19484370105.